[Research Paper] 대한금속 · 재료학회지 (*Korean J. Met. Mater.*), Vol. 60, No. 12 (2022) pp.919-925
DOI: 10.3365/KJMM.2022.60.12.919

Electrical, Thermal, and Thermoelectric Transport Properties of Se-doped Polycrystalline Re_2Te_5

Se Woong Lee[1,†], Okmin Park[1,†], Hyun-Sik Kim[1], Won-Seon Seo[2], and Sang-il Kim[1,*]

[1]*Department of Materials Science and Engineering, University of Seoul, Seoul 02504, Republic of Korea*
[2]*Department of Materials Science and Engineering, Yonsei University, Seoul 03722, Republic of Korea*

Abstract: Re_2Te_5 is considered a potential thermoelectric material because of its intrinsically low thermal conductivity, due to its complex crystal structure. Herein, a series of Se-doped Re_2Te_5 ($Re_2Te_{5-x}Se_x$, x = 0, 0.2, 1, and 2) samples were synthesized, and their electrical and thermal transport properties were investigated. Pure orthorhombic Re_2Te_5 phases were successfully synthesized without any impurities for all compositions, and the continuous decrease in the calculated lattice parameters confirmed the substitution of Se atoms at the Te sites. A maximum power factor of 0.135 mW/mK^2 was achieved for the sample with x = 0.2 at 880 K, mainly due to the increase in carrier concentration and electrical conductivity. The lattice thermal conductivity significantly decreased for all doped samples, which was attributed to the point defect phonon scattering caused by Se doping. The thermoelectric figure of merit, zT reached a maximum value of 0.20 at 880 K for $Re_2Te_{4.8}Se_{0.2}$ (x = 0.2) sample, which was approximately 22% higher than that of the pristine Re_2Te_5 sample. The weighted mobility, quality factor, and expected zT were calculated to evaluate the optimization of the power factor and zT.

(Received 17 June, 2022; Accepted 7 September, 2022)

Keywords: thermoelectric, doping, Re_2Te_5

1. INTRODUCTION

Numerous studies on eco-friendly energy-production technologies have been conducted in various fields [1]. In particular, thermoelectric technology can be used for reversible energy conversion—from heat to electricity based on the Seebeck and Peltier effects, respectively [2,3]. Thermoelectric performance is evaluated using the dimensionless thermoelectric figure of merit, $zT = S^2\sigma T/\kappa_{tot}$, where S, σ, κ_{tot} and T are the Seebeck coefficient, electrical conductivity, total thermal conductivity, and absolute temperature, respectively. Generally, κ_{tot} is divided = κ_{ele} and κ_{latt}, where κ_{ele} and κ_{latt} are electrical and lattice thermal conductivities, respectively. The most important goal of research on thermoelectric materials is to enhance zT. However, κ_{ele} and σ are closely related to each other according to the Wiedemann-Franz law ($\kappa_{ele} = L \cdot \sigma \cdot T$, where L is the Lorenz number) [4]; consequently, enhancing zT is challenging. Therefore, zT can be improved by either increasing the power factor ($S^2\sigma$, PF) or by decreasing κ_{tot}. Skutterudites are typical thermoelectric materials with high PF. $CoSb_3$-based skutterudites have a relatively high κ_{tot} of 3 W/mK or more and a high PF of approximately 5 mW/mK^2 [5]. Skutterudites show excellent thermoelectric performance at high temperatures, but relatively poor performance at low temperatures. Therefore, skutterudites are unsuitable for wearable devices or vehicle applications. The most effective strategy for improving zT at low temperatures is to reduce κ_{tot} [6,7]. Chalcogenides have a very low κ_{tot} owing to their weak van der Waals bonding between atomic layers; thus, they can be potential thermoelectric materials with a high zT even at room temperature [8].

Chalcogenides are being actively studied as modules for various devices such as wearable devices and generators for vehicles [9,10]. Defect engineering, such as doping and nanostructuring, is an effective approach for reducing κ_{latt} by

†These authors contributed equally to this work.
- 이세웅: 학부과정, 박옥민: 석사과정, 서원선: 연구교수, 김현식·김상일: 교수
**Corresponding Author:* Sang-il Kim
[Tel: +82-6490-2414, E-mail: sang1.kim@uos.ac.kr]

increasing point-defect phonon scattering [11-13]. This strategy has been adopted in many studies to enhance zT in chalcogenides [13-17]. Rhyee et al. reported that $In_4Se_{2.35}$ exhibited a very high zT value of 1.48 at 705 K via self-doping by Se deficiency [13]. Qin et al. synthesized Mn-doped $Bi_{0.5}Sb_{1.5}Te_3$ and a maximum zT of ~1.3 was achieved for $Mn_{0.0075}Bi_{0.5}Sb_{1.4925}Te_3$ at 430 K [15].

However, the thermoelectric performance of rhenium chalcogenide compounds has not been extensively investigated. According to density functional theory calculations by Hafeez et al. [18], ReS_2 and $ReSe_2$ have different band gaps:1.58 eV (1.50 eV) for monolayer (bulk) ReS_2 and 1.32 eV (1.26 eV) for monolayer (bulk) $ReSe_2$. Sreeparvathy reported that ReX_2 (X = S and Se) has flat bands aligned in both the valence and conduction bands, which contribute to the enhancement of S [19]. Sreeparvathy also showed that ReS_2 has the potential to have a large S of 540-600 μV/K at 300 K. Re_2Te_5, a rhenium chalcogenide, does not have a layered structure but has a complex orthorhombic (space group: Pbca [61]) crystal structure with 84 atoms ([Re_{24}] and [Te_{60}]) per unit cell. These atoms exhibit a cluster-type Chevrel phase, with [Re_6] surrounded by [Te_8] [20-22].

One of the structural properties of the Chevrel phase is the presence of four large vacancies. This causes scattering of phonons, effectively reducing κ_{latt}. Inevitably, κ_{tot} of Re_2Te_5 is 1.3 W/mK which is as low as that of chalcogenides which have layered structures [21]. Further, Caillat et al. reported that rattling was observed in elements doped into vacancies, resulting in reduced κ_{tot} due to increasing phonon scattering [23]. Therefore, the application of defect engineering to Re_2Te_5 is a reasonable approach for improving thermoelectric performance.

In this study, the thermoelectric transport properties of Se-doped Re_2Te_5 samples were investigated. We synthesized a series of $ReTe_{5-x}Se_x$ (x = 0, 0.2, 1, and 2) samples. The electrical and thermal transport properties of the samples were investigated, and Hall measurements were conducted to analyze the electrical transport properties of the samples in detail. The density-of-state effective mass was calculated from the measured parameters. zT was evaluated to determine the optimum composition for Se-doped Re_2Te_5.

2. EXPERIMENTAL

A series of $Re_2Te_{5-x}Se_x$ (x = 0, 0.2, 1, and 2) samples were stoichiometrically synthesized using a conventional solid-state reaction process. High-purity element Te (99.999%), Se (99.999%), and Re (99.999%) powders were mixed and loaded in a vacuum quartz tube. The loaded vacuum quartz tube was then heated to 950°C for 6 hours and then maintained for 70 hours. After heating, the samples were cooled to room temperature in a furnace. The synthesized Se-doped Re_2Te_5 samples were pulverized into powder by high-energy ball milling (SPEX 8000D, SPEX). The powder samples were placed in graphite molds and cold-pressed to form the green bodies. The samples were sintered using spark plasma sintering (SPS-1030, Sumitomo Coal Mining Co., Ltd.) under vacuum at 850°C for 10 min under 70 MPa. The crystal structures of the samples and the presence of impurities were identified using X-ray diffraction (XRD, D8 Discover, Bruker) analysis. Furthermore, σ and S were measured simultaneously using a thermoelectric-property measurement system (ZEM-3, Advanced-Riko) in the temperature range of 300-880 K in a He atmosphere. The error margins for σ and S were less than 3% and 5%, respectively.

The Hall carrier concentrations (n_H) and Hall carrier mobilities (μ_H) were measured using a Hall measurement system (HMS5300, Ecopia) under a 0.548 T magnetic field. The κ_{tot} value of each sample was calculated using the density (ρ_s), heat capacity (C_p), and thermal diffusivity (α). ρ_s was considered to be the theoretical density of orthorhombic Re_2Te_5 (8.423 g/cm^3 [2]). The C_p of each sample was measured by differential scanning calorimetry (DSC8000, Perkin Elmer). The α value of each sample was measured by laser flash analysis (LFA457, Netzsch). The error margin for α was less than 7%. The zT values of the samples were calculated based on measured data.

3. RESULTS AND DISCUSSION

Figures 1(a) and 1(b) show the XRD patterns and calculated lattice parameters of the series of $Re_2Te_{5-x}Se_x$ (x = 0, 0.2, 1, and 2) samples, respectively. As shown in Figure

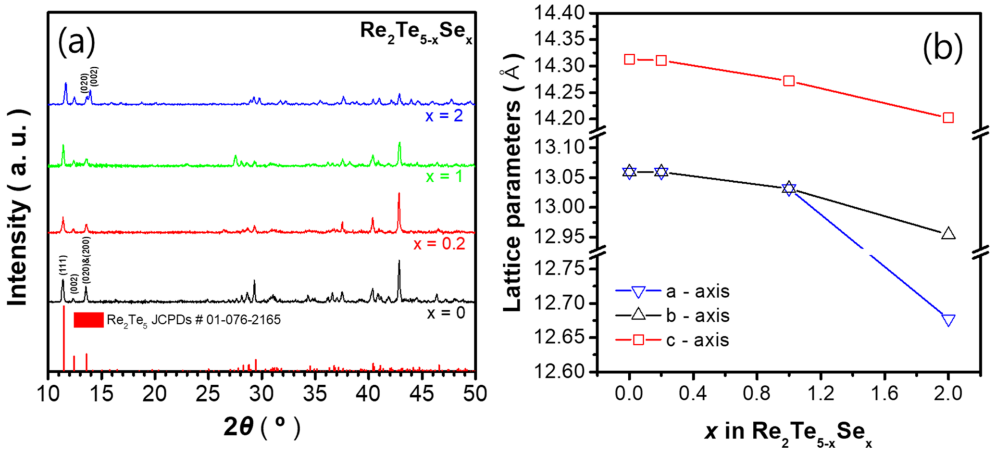

Fig. 1. (a) XRD patterns of the series of $Re_2Te_{5-x}Se_x$ (x = 0, 0.2, 1, and 2) samples. (b) Lattice parameters calculated from the XRD patterns.

1(a), single orthorhombic Re_2Te_5 phases were synthesized without impurities. The (200) and (020) diffraction peaks for the samples with x = 0, 0.2, and 1 appeared as a single peak, and the calculated lattice parameters, a and b of these samples were almost identical. However, for the sample with x = 2, the (200) and (020) peaks were separated. Therefore, the calculated lattice parameters, a and b for x = 2 exhibited significantly different values of 12.68 and 12.95 Å, respectively. The lattice parameters along the three axes gradually decreased with increasing Se doping content, which is attributed to the difference in ionic radii between Se^{2-} (184 pm) and Te^{2-} (207 pm). Therefore, this result confirms that Se atoms were successfully substituted at Te sites.

Figure 2 shows the thermoelectric transport properties measured perpendicular to the pressing axis. As shown in Figure 2(a), σ for the samples with x = 0, 0.2, 1, and 2 were 0.106, 0.112, 0.020, and 0.005 S/cm at 300 K, respectively. All the samples exhibited typical semiconductor behavior, and σ increased to 33.74, 36.71, 3.88, and 2.25 S/cm at 880 K for $Re_2Te_{5-x}Se_x$ with x = 0, 0.2, 1, and 2, respectively. The maximum σ value was observed for $Re_2Te_{5-x}Se_x$ with x = 0.2. Figure 2(b) shows the temperature dependence of S for the samples. At 300 K, the S values were 574, 497, 424, and 299 μV/K for $Re_2Te_{5-x}Se_x$ with x = 0, 0.2, 1, and 2, respectively; at 300 K S decreased gradually with increasing x.

Generally, the magnitude of S increases when σ decreases because of the trade-off relationship between S and σ. However, the S of the samples with x = 1 and 2 at 300 K decreased despite the decrease in σ of these samples. This result can be explained by the bipolar effect. The samples with x = 1 and 2 initially increased with T and then decreased following their maximum values at approximately 580 K, suggesting that bipolar excitation dominates the transport

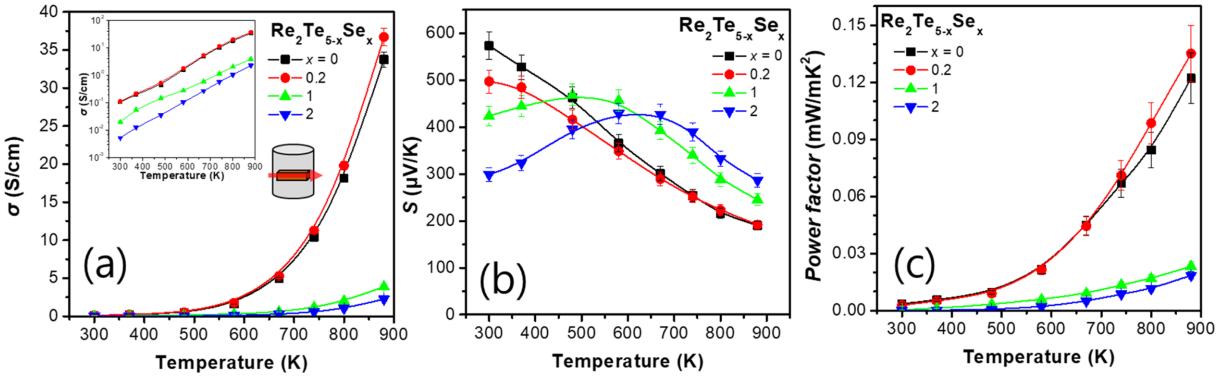

Fig. 2. (a) σ, (b) S, and (c) PF as a function of the temperature for the samples. The inset of (a) shows σ as a function of the temperature in a logarithmic scale.

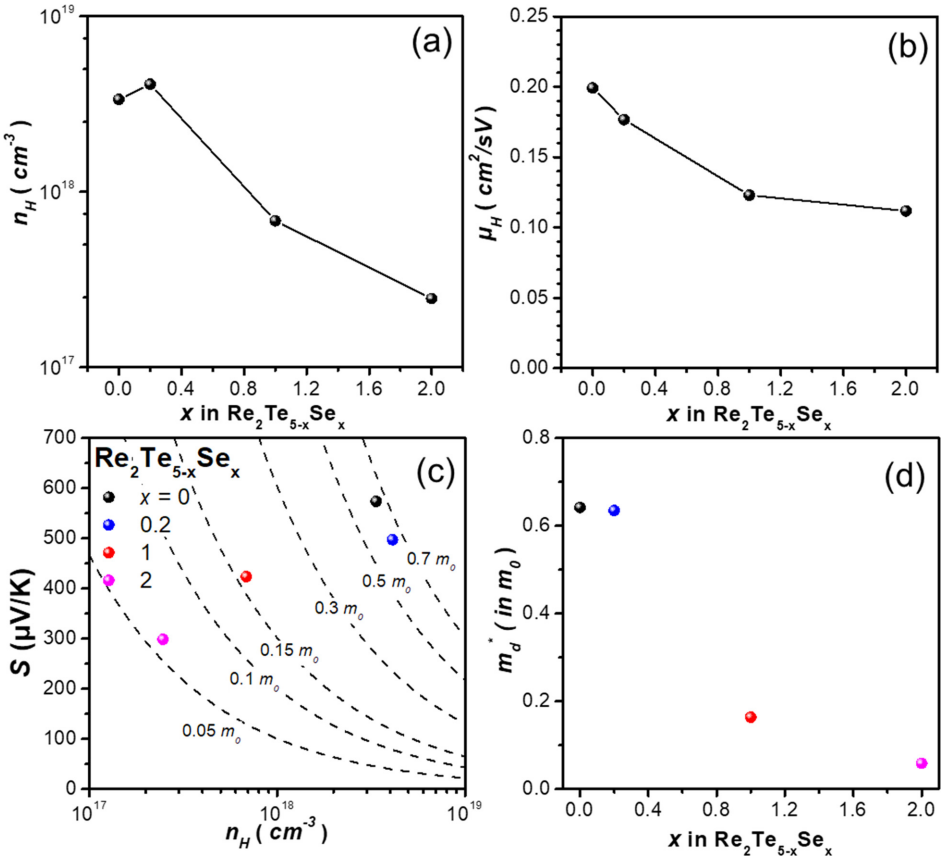

Fig. 3. (a) n_H and (b) μ_H of the samples at 300 K. (c) S as a function of the measured n_H (Pisarenko plot) at 300 K. (d) m_d^* as a function of x in $Re_2Te_{5-x}Se_x$ (x = 0, 0.2, 1, and 2).

[25]. Therefore, the relationship between the measured S completely reversed at 880 K; the values of S were 190, 192, 245, and 286 for x = 0, 0.2, 1, and 2, respectively at 880 K.

The PF values of the samples calculated from the measured σ and S values are shown in Figure 2(c). The PF values of the samples with x = 0 and 0.2 are very similar up to 670 K, but at T > 670 K, the PF value of the sample with x = 0.2 is higher than that of the sample with x = 0. Therefore, a maximum PF of 0.135 mW/mK^2 was achieved for x = 0.2 at 880 K. However, the samples with x = 1 and 2 exhibited very low PF values of 0.023 and 0.019 mW/mK^2 at 880 K, respectively. The decrease in PF for these samples is attributed to the reduction in σ and the small increase in S due to the amplified bipolar effect.

Figures 3(a) and 3(b) show the measured electrical transport properties of the samples at 300 K. The n_H value marginally increased from 3.37 × 10^{18} cm^{-3} to 4.11 × 10^{18} cm^{-3} when a small amount of Se (~0.03 at. %) was doped to pristine Re_2Te_5 sample. However, n_H decreased with a further increase in Se content. The μ_H values of the samples measured at 300 K were 0.20, 0.18, 0.12, and 0.11 cm^2/Vs for x = 0, 0.2, 1, and 2, respectively. The μ_H values decreased gradually as the Se content increased. The increase in σ for x = 0.2 and the decrease in σ for x = 1 and 2, were due to the improved n_H for the sample with x = 0.2, and the reduced n_H and μ_H for the samples with x = 1 and 2.

S as a function of n_H at 300 K is plotted for the series of samples (Pisarenko plot) in Figure 3(c). The dotted lines in Figure 3(c) indicate the contours of the density-of-state effective mass (m_d^*, expressed with respect to the free electron mass, m_0) according to the Mott relationship [26].

$$S = \frac{8\pi^2 k^2}{3eh^2}\frac{\pi}{3n}^{2/3} m_d^* T \quad (1)$$

where h, e, and k are the Planck's constant, elementary charge, and Boltzmann constant, respectively. Figure 3(d)

shows the change in m_d^* of the $Re_2Te_{5-x}Se_x$ (x = 0, 0.2, 1, and 2) samples with respect to x. As the Se content increased, the m_d^* value gradually decreased. The m_d^* values of the samples were 0.64, 0.63, 0.16, and 0.06 m_0 for the samples with x = 0, 0.2, 1, and 2, respectively.

Figure 4(a) shows the plot of κ_{tot} vs temperature for the $Re_2Te_{5-x}Se_x$ (x = 0, 0.2, 1, and 2) samples. The measured κ_{tot} value of the undoped sample gradually decreased with T from 1.33 to 0.59 W/mK up to 740 K, but then increased to 0.66 W/mK at 880 K. The κ_{tot} values of the doped samples were significantly low (below ~0.85 W/mK), and notably, the samples with x = 1 and 2 exhibited very low κ_{tot} values of 0.23-0.53 W/mK. Figure 4(b) shows the temperature dependence of κ_{ele} of the samples, and the κ_{ele} values

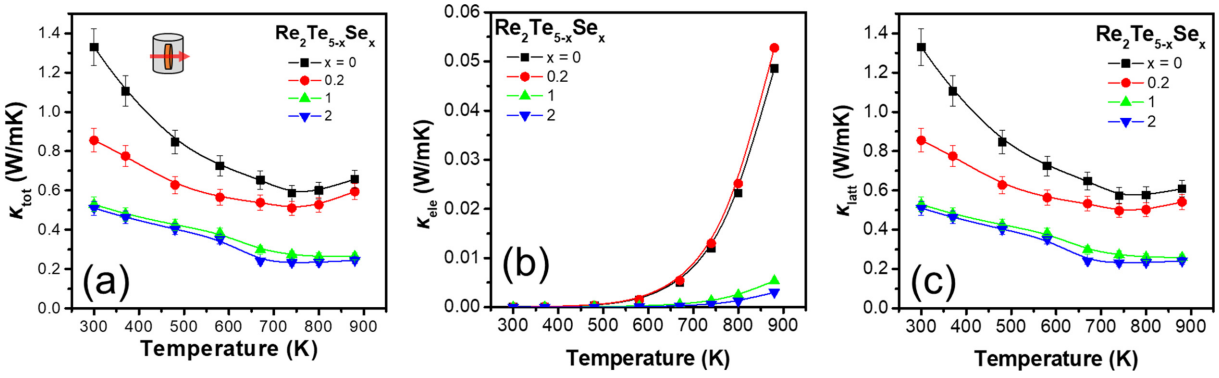

Fig. 4. (a) κ_{tot}, (b) κ_{ele}, and (c) κ_{latt} as a function of the temperature for the samples.

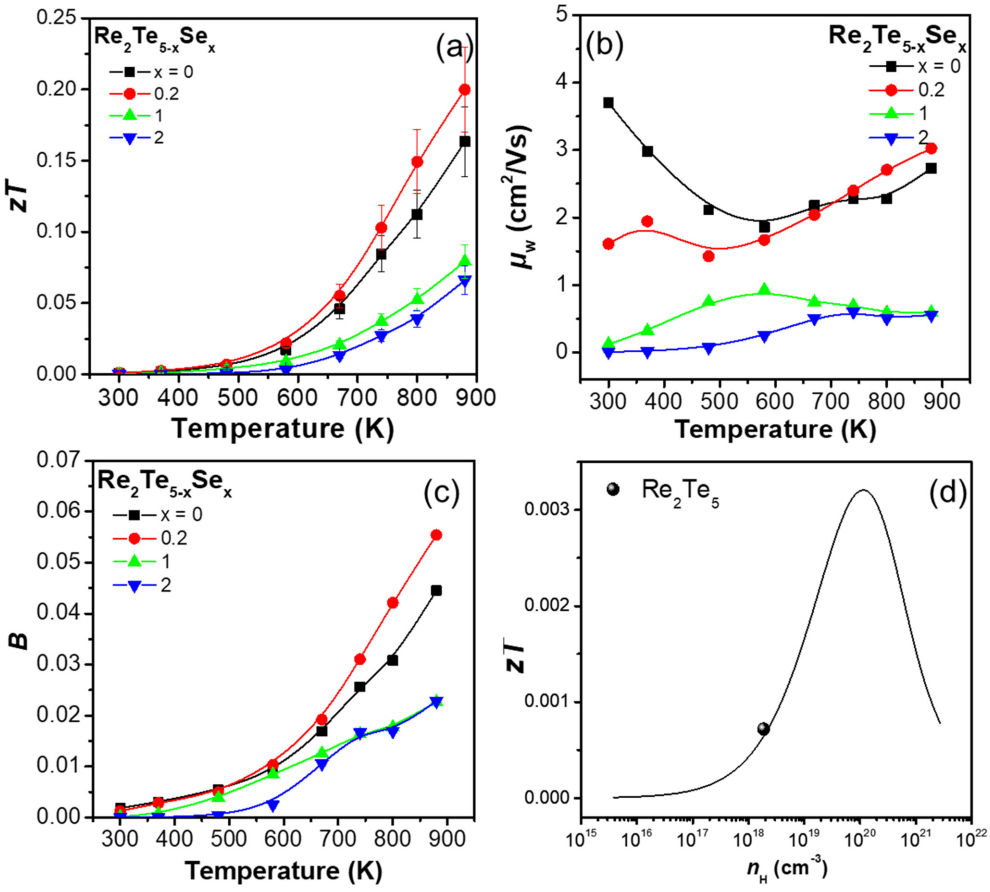

Fig. 5. (a) zT, (b) μ_w, and (c) B as a function of the temperature for the samples. (d) Predicted zT of Re_2Te_5 at 300 K calculated based on the single parabolic band model as a function of n_H.

exhibited a trend similar to that of the σ values. However, the influence of κ_{ele} on κ_{tot} was marginal, because the measured σ was less than 50 S/cm. Consequently, the κ_{latt} values were almost identical to the κ_{tot} values, as shown in Figure 4(c). Further, κ_{latt} gradually decreased with increasing Se content over the entire temperature range; this was attributed to the point defect phonon scattering by Se doping.

The gradual decrease in lattice parameters *a*, *b*, and *c* suggests an increase in lattice distortion, which leads to a decrease in κ_{latt}. Furthermore, the scattering parameters are proportional to the difference in mass (ΔM) in the point-defect scattering mechanism [27]. Therefore, the difference between the atomic masses of Te (127.6 u) and Se (79.0 u) also contributed to the decrease in κ_{latt}.

Next, the *zT* values were calculated using the measured σ, *S*, and κ_{tot} values of the samples (Figure 5(a)). The error margin for *zT* was less than 15%. The highest *zT* value of 0.20 was achieved for the sample with x = 0.2 at 880 K, which is ~22% higher than that of the pristine Re_2Te_5 sample. The *zT* enhancement for x = 0.2 was attributed to the marginal increase in *PF* and decrease in κ_{tot}. However, the other doped samples (x = 1 and 2) exhibited reduced *zT* values because of the significant decrease in *PF*, despite the very low κ_{tot} values.

Figure 5(b) shows the weighted mobility (μ_w) as a function of the temperature for the samples. μ_w is proportional to the maximum *PF* that a sample can reach when n_H is optimized. The μ_w value of each sample was calculated from the measured σ and *S*; μ_w can be obtained from a simple analytical form that approximates the exact Drude-Sommerfeld free-electron model given in Equation (2) for $|S|$ > 20 μV/K [28].

$$\mu_w = \frac{3h^3\sigma}{8\pi e(2m_e kT)^{3/2}}\left[\frac{\exp\left[\frac{|S|}{k/e}-2\right]}{1+\exp\left[-5\left(\frac{|S|}{k/e}-1\right)\right]}+\frac{\frac{3}{\pi^2}\frac{|S|}{k/e}}{1+\exp\left[5\left(\frac{|S|}{k/e}-1\right)\right]}\right] \quad (2)$$

where m_e is the mass of the electron. The calculated μ_w values at 880 K were 2.73, 3.03, 0.59, and 0.56 cm^2/Vs for x = 0, 0.2, 1, and 2, respectively. The μ_w values increased at x = 0.2, and then decreased with increasing x, which is in agreement with the *PF* trend at 880 K. Therefore, the *PF* of the sample with x = 0.2 can be further improved by appropriate n_H tuning. In addition, μ_w is closely related to m_d^* as shown in Equation (3) [29].

$$\mu_w = \mu_0 \cdot \left(\frac{m_d^*}{m_0}\right)^{3/2} \quad (3)$$

where μ_0 is the non-degenerate mobility. The μ_w values of the samples at 300 K were 3.70, 1.61, 0.12, and 0.08 cm^2/Vs for x = 0, 0.2, 1, and 2, respectively. The μ_w values at 300 K decreased with x, which can also be observed in the m_d^* trend.

Figure 5(c) shows the dimensionless thermoelectric quality factor (*B*) of each sample, calculated from μ_w and κ_{latt}. *B* was calculated using Equation (4) [28]:

$$B = \left(\frac{k}{e}\right)^2 \frac{8\pi e(2m_e kT)^{3/2}}{3h^3}\cdot\frac{\mu_w}{\kappa_{latt}}T \quad (4)$$

B is related to the maximum *zT* that a material can achieve when n_H is optimized. The general trend of *B* closely followed that of *zT*: *B* increased at x = 0.2, and decreased with a further increase in Se content. Figure 5(d) shows the plot of the expected *zT* of pristine Re_2Te_5 as a function of n_H at 300 K using a single parabolic band model. The parabolic line in Figure 5(d) was calculated using Equation (5) [29].

$$zT = \frac{\left(\frac{k_B}{e}\right)^2\left(\frac{2F_1(\eta)}{F_0(\eta)}-\eta\right)^2\left(\frac{8\pi e^2(2m_d^* k_B T)^{3/2}}{3m_d^* h^3\kappa_{latt}}\tau_{0,ac}\right)F_0(\eta)T}{1+\left(\frac{k_B}{e}\right)^2\left[\frac{3F_1(\eta)}{F_0(\eta)}-\left(\frac{2F_1(\eta)}{F_0(\eta)}\right)^2\right]\left(\frac{8\pi e^2(2m_d^* k_B T)^{3/2}}{3m_d^* h^3\kappa_{latt}}\tau_{0,ac}\right)F_0(\eta)T} \quad (5)$$

where $F_x(\eta)$ (η is the reduced electrochemical potential) and τ_{ac} are the Fermi integral and relaxation time of acoustic phonon scattering, respectively.

Therefore, maximum *zT* can be achieved when n_H is ~10^{20} cm^{-3}. Accordingly, the *zT* of Re_2Te_5 can be substantially enhanced by appropriate cation doping, such as Zr^{4+}, Sn^{4+} and Hf^{4+}, in Re^{5+}-site, considering the significant decrease in κ_{tot} due to Se doping.

4. CONCLUSIONS

A series of $Re_2Te_{5-x}Se_x$ (x = 0, 0.2, 1, and 2) polycrystalline samples were prepared to investigate their electrical and thermal transport properties. Pure orthorhombic Re_2Te_5

phases were synthesized without any impurities, and the lattice parameters *a*, *b*, and *c* gradually decreased with increasing Se content, confirming the substitution of Se atoms at the Te sites. A maximum power factor of 0.135 mW/mK^2 was obtained for the sample with $x = 0.2$ at 880 K, predominantly due to the increase in the n_H and σ. The lattice thermal conductivity significantly decreased with increasing Se content, which was attributed to the point defect phonon scattering by Se doping. Further, zT reached a maximum value of 0.20 at 880 K for the $Re_2Te_{4.8}Se_{0.2}$ ($x = 0.2$) sample, an enhancement of approximately 22% compared to the pristine Re_2Te_5 sample. The single parabolic band model predicted that zT can be further improved by appropriate n_H tuning.

ACKNOWLEDGEMENTS

This work was supported by the National Research Foundation of Korea (NRF-2019R1C1C1005254, NRF-2019R1A6A1A11055660, NRF-2022R1F1A1063054).

REFERENCES

1. M. P. Cenci, T. Scarazzato, D. D. Munchen, P. C. Dartora, H. M. Veit, A. M. Bernardes, and P. R. Dias, *Adv. Mater. Technol.* **7**, 2001263 (2022).
2. L. E. Bell, *Science* **321**, 1457 (2008).
3. J. Flipse, F. L. Bakker, A. Slachter, F. K. Dejene, and B. J. van Wees, *Nat. Nanotechnol.* **7**, 166 (2012).
4. Z. Lin and L. V. Zhigilei, *Appl. Surf. Sci.* **253**, 6295 (2007).
5. Z.-Y. Liu, J.-L. Zhu, X. Tong, S. Niu, and W.-Y. Zhao, *J. Adv. Ceram.* **9**, 647 (2020).
6. H. J. Cho, H.-S. Kim, and S.-I. Kim, *Korean J. Met. Mater.* **57**, 673 (2019).
7. K. H. Lee, M. W. Oh, H. S. Kim W. H. Shin, K. Lee, J. H. Lim, J. Kim, and S.-I. Kim, *Inorg. Chem. Front.* **6**, 1475 (2019).
8. M. M. Alsalama, H. Hamoudi, A. Abdala, Z. K. Ghouri, and K. M. Youssef, *Rev. Adv. Mater. Sci.* **59**, 371 (2020).
9. X. Zhao, C. Zhao, Y. Jiang, X. Ji, F. Kong, T. Lin, H. Shao, and W. Han, *J. Power Sources* **479**, 229044 (2020).
10. S. Harish, D. Sivaprahasam, B. Jayachandran, R. Gopalan, and G. Sundararajan, *Energy Convers. Manag.* **232**, 113900 (2021).
11. S. Feihong, Z. Yanyan, M. Lei, L. Chengyan, G. Jie, W. Xiaoyang, L. Pengfei, Y. Kenta, and C. Huanfu, *ACS Appl. Mater. Interfaces* **12**, 8385 (2020).
12. O. Park, T. Kim, S. W. Lee, H. Kim, W. H. Shin, J. U. Rahman, and S. Kim, *Korean J. Met. Mater.* **60**, 315 (2022).
13. J.-S. Rhyee, K. H. Lee, S. M. Lee, E. Cho, S. I. Kim, E. Lee, Y. S. Kwon, J. H. Shim, and G. Kotliar, *Nature* **459**, 965 (2009).
14. S. Kim, J. Bang, J. An, S. Hong, G. Bang, W. H. Shin, T. W. Kim, and K. Lee, *J. Alloy Compd.* **868**, 159161 (2021).
15. H. Qin, Y. Liu, Z. Zhang, Y. Wang, J. Cao, W. Cai, Q. Zhang, and J. Sui, *Mater. Today Phys.* **6**, 31 (2018).
16. R. Juneja, T. Pandey, and A. K. Singh, *Chem. Mater.* **29**, 3723 (2017).
17. H. J. Cho, H. S. Kim, and S. I. Kim, *Korean J. Met. Mater.* **57**, 673 (2019).
18. M. Hafeez, L. Gan, A. S. Bhatti, and T. Zhai, *Mater. Chem. Front.* **1**, 1917 (2017).
19. P. C. Sreeparvathy, *Ph. D. Thesis*, Indian Institue of Technology Hyderabad, India (2019).
20. S. G. Kozlova, S. P. Gabuda, and V. V. Terskikh, *Solid State Nucl. Mag.* **25**, 72 (2004).
21. C. Godart, A. P. Gonçalves, E. B. Lopes, and B. Villeroy, *Properties and Applications of Thermoelectric Materials*, Springer, Dordrecht, Nederland (2009).
22. T. Caillat and J.-P. Fleurial, *XVI ICT'97. Proceedings ICT'97. 16th International Conference on Thermoelectrics (Cat. No. 97TH8291),* pp.446-453, Institute of Electrical and Electronics Engineers, New York, USA (1997).
23. T. Caillat, J.-P. Fleurial, and G. J. Snyder, *Solid State Sci.* **1**, 535 (1999).
24. F. Klaiber, W. Petter, and F. Hulliger, *J. Solid State Chem.* **46**, 112 (1983).
25. Z. Guo, K. Song, Z. Yan, P. Sun, X. Tan, G. Wu, Q. Zhang, G.-Q. Liu, B. Yu, and J. Jiang, *Chem. Eng. J.* **426**, 131853 (2021).
26. A. F. Ioffe, *Physics of Semiconductors*, Academic Press, New York (1960).
27. B. R. Oritz, H. Peng, A. Lopez, P. A. Parilla, S. Lany, and E. S. Toberer, *Phys. Chem. Chem. Phys.* **17**, 19410 (2015).
28. G. J. Snyder, A. H. Snyder, M. Wood, R. Gurunathan, B. H. Snyder, and C. Niu, *Adv. Mater.* **32**, 2001537 (2020).
29. M. Kim, S.-I. Kim, S. W. Kim, H.-S. Kim, and K. H. Lee, *Adv. Mater.* **33**, 2005931 (2021).